PERGAMON

Journal of Structural Geology 25 (2003) 79–90

JOURNAL OF STRUCTURAL GEOLOGY

www.elsevier.com/locate/jsg

Three-dimensional horizon reconstruction from outcrop structural data, restoration, and strain field of the Baisahi anticline, Western Nepal

Laurent Husson[a,*], Jean-Louis Mugnier[b,1]

[a]*Ecole Normale Supérieure de Lyon, UMR CNRS 5570, 46 Allée d'Italie, 69364 Lyon cedex 07, France*
[b]*LGCA, UPRESA CNRS 5025, 1381 Rue de la piscine, BP 53, 38041 Grenoble cedex 9, France*

Received 28 February 2001; received in revised form 7 March 2002; accepted 14 March 2002

Abstract

Within many fold and thrust belts, preservation of bed thickness is generally assumed during deformation. A three-dimensional (3D) reconstruction method is proposed from outcrop structural data. This technique accounts for along-strike thickness variations. By a series of 3D spatial projections of dip and strike data, the thickness of strata from any point at the ground surface to reference horizons on stratigraphic columns can be calculated across-strike and projected along the poles of the associated strata, providing sets of dots in space, which represent folded horizons.

The technique is applied to the Baisahi antiform, located on the frontal Subhimalayan thrust. An along-strike deformation gradient is evidenced by two-dimensional cross-section balancing, which shows a passive-roof duplex structure. The 3D geometry of the roof is reconstructed, allowing other approaches such as unfolding to be done. The residual strain field induced by restoration shows distortion features, which are interpreted as internal strain due to the propagation of the fault.

Keywords: 3D reconstruction; Unfolding; Strain; Passive roof duplex; Subhimalayan zone

1. Introduction

The characterization of fold and thrust belt structures is of major relevance world-wide, for both industrial and academic interests. Reconstruction of the three-dimensional (3D) geometry of complex structures still constitutes a major goal for structural geology. The structural description of these areas can be poorly constrained when these zones are remote; in these cases, subsurface geometries are badly documented due to very widely spaced seismic and well data. Two-dimensional (2D) cross-section balancing (Dahlstrom, 1969; Boyer and Elliott, 1982; Woodward et al., 1985) led to major progress in the interpretation of structures at depth. The purpose of this study is to present an original 3D reconstruction method from outcrop structural data. This technique allows the 3D shape of structures to be evaluated in both their eroded and buried parts, only from the measured attitudes of bedding at surface level.

An application to the Baisahi anticline, in the Subhimalayan range of Western Nepal, is presented. Cross-section balancing helps to estimate the geometry and kinematics of the Baisahi structure. The high resolution structural map (Kayastha et al., 1999) provides the data necessary to undertake reconstruction of the Baisahi antiform in 2D and ultimately in 3D. Additionally, unfolding of a 3D reconstructed horizon is used to constrain the evolution of the structure.

The Subhimalayan range of Western Nepal is a southward tapering wedge of syn-orogenic sediments, located in the Himalayan foothills. It is made of several south-verging slices of coarsening upward molasse. Constant bed thickness is a general assumption in this area (e.g. Schelling and Arita, 1991; Mugnier et al., 1992; Schelling, 1992; Powers et al., 1998) and flexural slip hypothesis has been successfully tested on active folding there (Lavé and Avouac, 2000). Moreover, the wedge only underwent a single N10 to N30 horizontal main shortening direction (Jouanne et al., 1999). Numerous structural data were acquired in this zone. Therefore this area is appropriate to apply the proposed 3D reconstruction technique.

2. Geological framework

2.1. Regional setting

The Subhimalayan range constitutes the southern

* Corresponding author. Fax: +33-4-7272-8677.
E-mail addresses: laurent.husson@ens-lyon.fr (L. Husson), mugnier@ ujf-grenoble.fr (J.-L. Mugnier).
[1] Tel.: +33-4-7651-4070; fax: +33-4-7651-4058.

0191-8141/02/$ - see front matter
PII: S0191-8141(02)00044-5

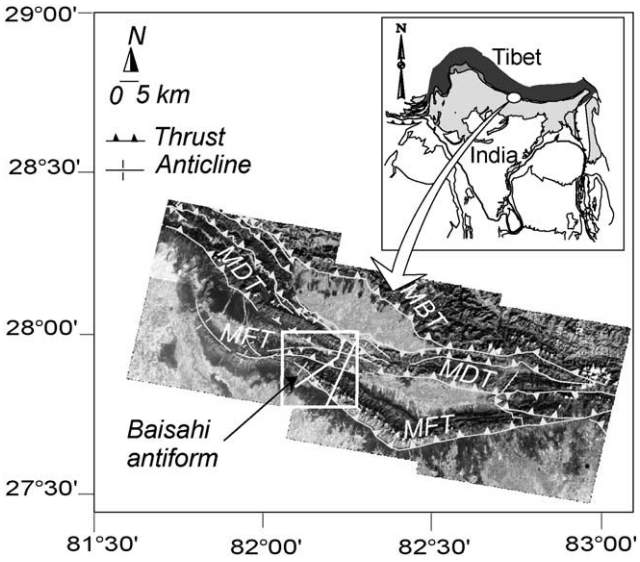

Fig. 1. SPOT spatial imagery and structural sketch of the study area. MFT: Main Frontal Thrust; MDT: Main Dun Thrust; MBT, Main Boundary Thrust. Box: Baisahi reconstructed antiform. Icon: location of the study area. White lines: location of cross-sections. © Cnes 1991—Spot Image Distribution.

foothills of the Himalayas, above the downflexed Indian lithosphere. It is a tectonic wedge of syn-orogenic sediments, fed by the foreland Indo-Gangetic alluvial plain. This wedge accommodates an important part of the Indo-Asian convergence of 50–55 mm/year (Molnar and Tapponnier, 1975; De Mets et al., 1990); shortening rates within the Subhimalayan wedge are estimated to be in the range of 17 ± 5 mm/year (Lyon-Caen and Molnar, 1985; Schelling, 1992; Jackson and Bilham, 1994; Peltzer and Saucier, 1996; Bilham et al., 1997; Mugnier et al., 1999). The Himalayan foothills consist of a few (3–5), mainly south-verging thrust sheets (e.g. Mascle et al., 1986; Leturmy, 1997; Powers et al., 1998), which characterize the thin-skinned pattern of deformation in this intracontinental wedge (Mugnier et al., 1992, 1999; Husson et al., 2002). The faults branch from a major décollement that dips 4–5° to the north (Galahaut and Chandler, 1992; Biswas, 1994; Raiverman et al., 1994). Shortening is accommodated by the Main Boundary Thrust (MBT) at the northern boundary with the Lesser Himalayas, the Main Frontal Thrust (MFT) to the south and the Main Dun Thrust (MDT) in between (Hérail and Mascle, 1980; Mugnier et al., 1992, 1998). The Subhimalayan range has been mainly described as fault propagation folds, duplexes, and north-dipping monoclines (e.g. Banks and Warburton, 1986; Mascle et al., 1986; Powers et al., 1998; Mugnier et al., 1999).

The stratigraphic sequence involved in shortening is primarily composed of coarsening upward molasse. The molasse, or Siwalik Group, is divided into three major units (e.g. Appel and Rosler, 1994): a distal facies of the Lower Siwaliks (LS1 and LS2, Middle Miocene); a wetland-type facies of the Middle Siwaliks 1 and 2 (MS1 and MS2, Upper Miocene); and a proximal facies of the Upper Siwaliks 1 and 2 (US1 and US2, Pliocene to Lower Pleistocene). These facies record the development and southward progradation of the Subhimalayan range (Hérail et al., 1987; Delcaillau, 1997). The basal décollement is located at the base of the Lower Siwaliks Fm. Duplexes are located below an additional décollement within the Lower Siwalik Fm (e.g. Leturmy, 1997; Mugnier et al., 1999).

2.2. The Baisahi antiform and Rapti syncline

The structure described herein is located at the western end of a MFT segment (Fig. 1), which varies along-strike from a north-dipping monocline at the east to a faulted ramp-fold to the west, and terminates as the Baisahi antiform. Thus, it represents the initial stage in the development of a ramp fold, a situation of major relevance for understanding the wedge tectonic regime and kinematics.

A structural map (Fig. 2) has been compiled from both field data and spatial imagery. Fieldwork provided attitudes of bedding along riverbed exposures. Processing of SPOT imagery (Principal Components Analysis and usual directional filters) allows horizons and contacts of the antiformal Baisahi structure to be correlated between the field transects defined by exposures in streambeds, up to its western closure.

The study area is bounded by the southernmost structural feature (MFT), which becomes blind westward; the corresponding tip point of the fault has been located using SPOT imagery and a 1:50,000 scale geological map (Shresta, personal communication). The Rapti syncline, located north of the Baisahi antiform, is offset on its northern edge by the Rapti reverse fault, which displays minor top-to-the-south displacement (Fig. 2). This fault bounds the analyzed structure to the north. Eastward, the reconstructed surface is arbitrarily limited by the 82°20′ meridian. The western edge of the study area is bounded by the periclinal closure, which displays local accommodation structures (minor thrusts and strike-slip faults) as the Baisahi and Rapti folds get increasingly more tightly oppressed between the blind MFT and the Rapti fault. Bedding data (avoiding the pericline) indicate that the structure is cylindrical on average although it can deviate from true cylindricity as the plunge oscillates around an average horizontal axis (Fig. 2).

Fig. 2. Structural map of the study area. Shaded areas are sampling bands for 3D horizon reconstruction, bold solid lines are reference horizons, dashed lines are location of cross-sections. LS: Lower Siwalik Fm.; MS: Middle Siwalik Fm.; US: Upper Siwalik Fm. The Baisahi anticline and Rapti syncline constitute the reconstructed structure. Box: Stereographic projections of outcrop structural data (without the western pericline area). The average cylindrical shape is evidenced by the distribution of the projected poles over a great circle.

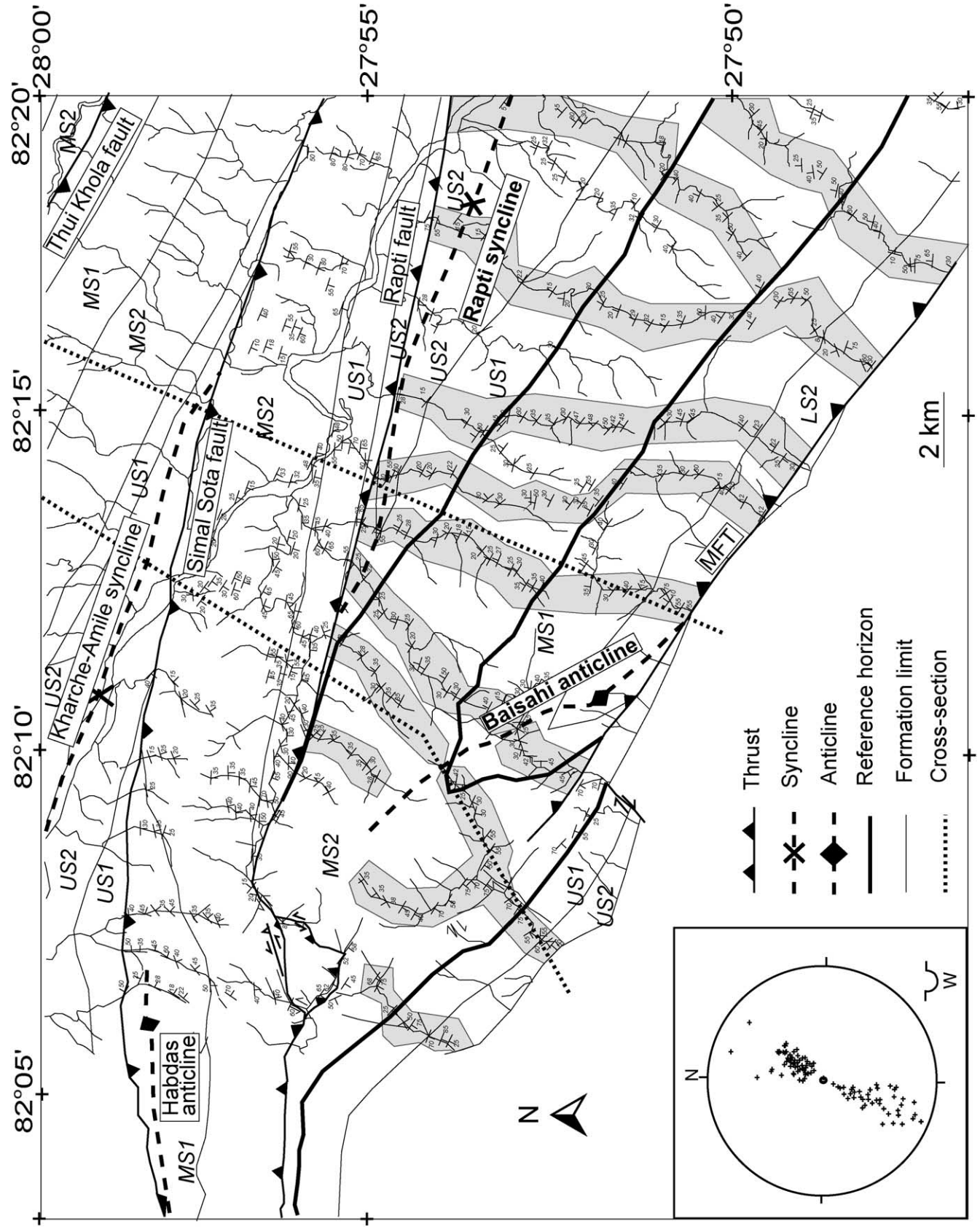
82°20'
82°15'
82°10'
82°05'
28°00'
27°55'
27°50'
Thui Khola fault
Kharche-Amile syncline
Simal Sota fault
Habdas anticline
Rapti fault
Rapti syncline
Baisahi anticline
MFT
MS1
MS2
US1
US2
LS2
2 km
N
Thrust
Syncline
Anticline
Reference horizon
Formation limit
Cross-section

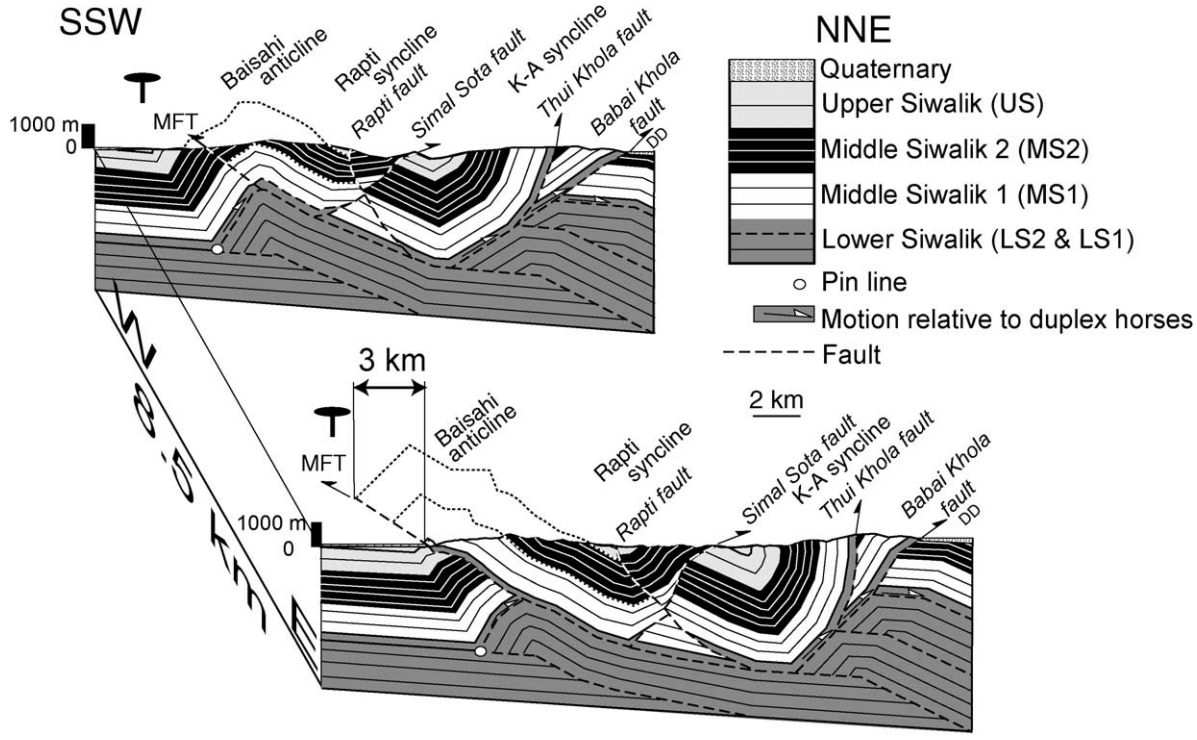

Fig. 3. Balanced cross-sections across the study area. Top: western section; bottom: eastern section. Dashed lines are décollement levels, dotted lines are 3D reconstructed horizons. MFT: Main Frontal Thrust; K.A. Syncline: Kharche–Amile Syncline; DD: Deukhuri Dang. The Thui Khola, Simal Sota and Babai Khola faults are the backthrusts for the passive-roof duplex. Location Fig. 2. The difference in offset between the sections indicates an apparent rotation of the roof of at least 20°.

Structural features in the vicinity of the field area include the Simal Sota and Thui Khola backthrusts in the north and the Kharche–Amile syncline, located between the Thui Khola and Simal Sota backthrusts (Fig. 2). North of the Thui Khola, the structures dip to the south and disappear beneath an alluvial basin (Dang Valley) overthrust by the Babai Khola backthrust. The backthrusts suggest that blind structural features might be hidden beneath the southern Baisahi anticline, stratigraphically within the LS unit.

The measured stratigraphic thickness from one flank to another along a section suggests that constant bed thickness is a correct assumption for 2D reconstruction. Moreover, flexural-slip is assumed to rule the deformation. Two balanced cross-sections have subsequently been constructed on the basis of constant bed lengths and thicknesses and 2D restorability (Dahlstrom, 1969; Woodward et al., 1985) assuming that the section is parallel to the regional displacement vector (Fig. 3). The basal décollement is assumed to gently dip northward at the base of the Lower Siwaliks unit. Such a décollement has already been documented by many authors within the Lower Siwalik Formation (e.g. Schelling and Arita, 1991; Schelling, 1992, Mugnier et al., 1992, 1994, 1999; Acharyya, 1994; Srivastava and Mitra, 1994; Ni and Barraganzi, 1996). The stratigraphic thicknesses are extrapolated from outcrops and estimates from the previous authors. The cross-sections (Fig. 3) are parallel to the average regional compression axis, i.e. between N10° and N30° (Mugnier et al., 1992, 1999; Jouanne et al., 1999). The azimuth of the folds axis is 130°, whereas the overall trend of the Subhimalayan range of Western Nepal is 100–110°. No compressive structure is observed further south, and we assume that shortening is limited southward by the MFT.

Cross-section balancing (Fig. 3) highlights that the base of the MS1 formation beneath the Rapti syncline is 1000–2000 m higher than beneath the Indo-Gangetic plain, indicating that it has been significantly uplifted by blind underlying structures. Moreover, the MFT itself is located close to the top of the LS formation. We interpret these observations as evidence for Lower Siwalik formation horses stacking beneath the Baisahi and Rapti folds. Two décollement levels are assumed to be present, at the base of the entire Siwalik Group and within the Lower Siwalik Fm (LS1/LS2 boundary). Unfortunately no subsurface data is currently available to confirm it. However, duplexes have been described previously, involving similar décollement levels (e.g. Schelling, 1992; Mugnier et al., 1994, 1999; Leturmy, 1997).

Following the assumptions stated above, a passive-roof duplex structure gives a balanced geometry. We are aware that contributions from ancient faults cannot be absolutely rejected to explain the uplift of the Rapti syncline by deforming the base of the young Siwalik Group, but it would not explain the location of the MFT close to the top of the Lower Siwalik formation. Many examples of

passive-roof duplexes have been documented world-wide, therefore emphasizing the widespread importance of these blind structures in thrust systems (Suppe, 1980; Price, 1981; Banks and Warburton, 1986; Boyer, 1986; Vann et al., 1986; Wines, 1990; Baby et al., 1992; Medwedeff, 1992; Leturmy, 1997; Mueller and Talling, 1997). Banks and Warburton (1986) defined these as duplexes "whose roof thrust has a backthrust sense and whose roof sequence remains stationary during foreland directed piggy-back style propagation of horses within the duplex". The duplex here involves horses mainly made of the Lower Siwalik LS1 formation; the tendency to form duplexes in the Subhimalayan range is described over the whole Siwalik range (e.g. Biswas, 1994; Mugnier et al., 1994; 1999; Leturmy, 1997). In our interpretation, the Simal Sota, Thui Khola and Babai Khola faults accommodate the passive reverse motion of the duplex roof. Westward, close to the Habdas anticline, the Simal Sota backthrust gradually exhumes deeper levels (up to the upper part of MS1), which indicates that this fault only has a minor throw (increasing westward).

We suggest that north of the Thui Khola fault, other LS duplex slices also associated with the Babai Khola backthrust are required, as shown in Fig. 3. However, as the structure is buried below the Quaternary Deukhuri Dang, the lack of data makes the geometrical interpretation at depth speculative north of the Babai Khola fault. These horses will not be discussed since they are not the focus of the study. The Rapti fault constitutes a late reverse fault with a strike-slip component (deduced from spatial imagery), crosscutting the core of the Rapti syncline. The emerging MFT itself also reflects the late stage evolution of the structure, as it branches off the roof thrust, and thereafter cuts the forelimb of the antiform as a synclinal breakthrough (Suppe and Medwedeff, 1990; Storti and Salvini, 1996). Hence, it post-dates the development of the underlying duplex structure. From terrace uplift (Leturmy, 1997; Lavé and Avouac, 2000), it has been shown that the MFT is the main thrust currently acting in the Siwaliks; it constitutes a discontinuous thrust at the front of the Himalayas (Husson et al., 2001). In the study area, a MFT segment terminates from east to west in the Baisahi anticline.

This stage is similar to the late stage of evolution of fault-propagation folds. The western cross-section displays no slip on the MFT, whereas the eastern one, 8.5 km east, shows a minimum slip of 3 km. It rises the problem of accommodating the difference of displacement between the mature eastern part and the immature western one. High shear strain or extension (Coward and Potts, 1983) are expected hinterland. The Wheeler Ridge, in California, has a very similar evolution (Medwedeff, 1992; Mueller and Talling, 1997), and presents geomorphic evidence for numerous tear faults accommodating the shear strain in this truly cylindrical structure. Another way to accommodate shear strain is to generate extension rather than tear faults.

3. 3D reconstruction methodology

We now describe how a 3D structure can be reconstructed from a simple data set comprising coordinates, height above sea level, strikes and dips of measured strata. This method is somehow close to the Busk reconstruction technique (Busk, 1929). The major assumptions of our horizon projection method are fairly common for fold and thrust belts analysis, generally exposed in 2D. A first order assumption is that bed thicknesses remain invariable during the folding event (flexural slip). Since the data are compiled along sections which are broadly perpendicular to strike, it is also assumed that over the distance required to compile the data along these 'band-sections', bed thickness is constant perpendicularly to the structural trend. These two assumptions imply 2D constant bed thickness across-strike during and after folding, for each independent section, from one fold limb to the other. However, our method accounts for lateral thickness variations along-strike. Each section is independent and has its own stratigraphic thicknesses. Folded structures are generally more elongated than large, and along-strike thickness variations can be found in many settings.

The required input data set contains structural measurements, defined by the absolute spatial coordinates of the datapoints and their strikes and dips. Although surface data are more likely to be used, well data or seismic data can be integrated. The denser the net of structural data, the more accurate the reconstructed surfaces will be. Since this method is based on 3D projections, the additional degree of freedom requires particularly tight data sets. However, the method also takes advantage of this because the 3D projections do not generate any distortion of the original measured data set: dips and strikes are compiled as they are acquired in the field, and are not extrapolated to lay within a vertical plane as it is in 2D. Processing of the digitized data sets provides the output data set for 3D modeling.

3.1. Stratigraphic thickness calculations

The general algorithm is described below:

(i) **Input**: coordinates, dip, strike datafiles for each sampling band (x_i,y_i,z_i,d_i,s_i).
(ii) Fold axis: vector coordinates and spatial location between each adjacent datapoints.
(iii) Trend and plunge of each fold axis.
(iv) Relative and cumulative stratigraphic thicknesses along each sampling band.
(v) Location of the reference horizon along the stratigraphic pole and spatial coordinates.
(vii) **Output**: (x'_i,y'_i,z'_i) dataset. Each dot belongs to the reference horizon.

Roman numbers refer to those given in the following paragraph. The initial data set (i) consists of points P_i defined by their coordinates, and a vector normal to the

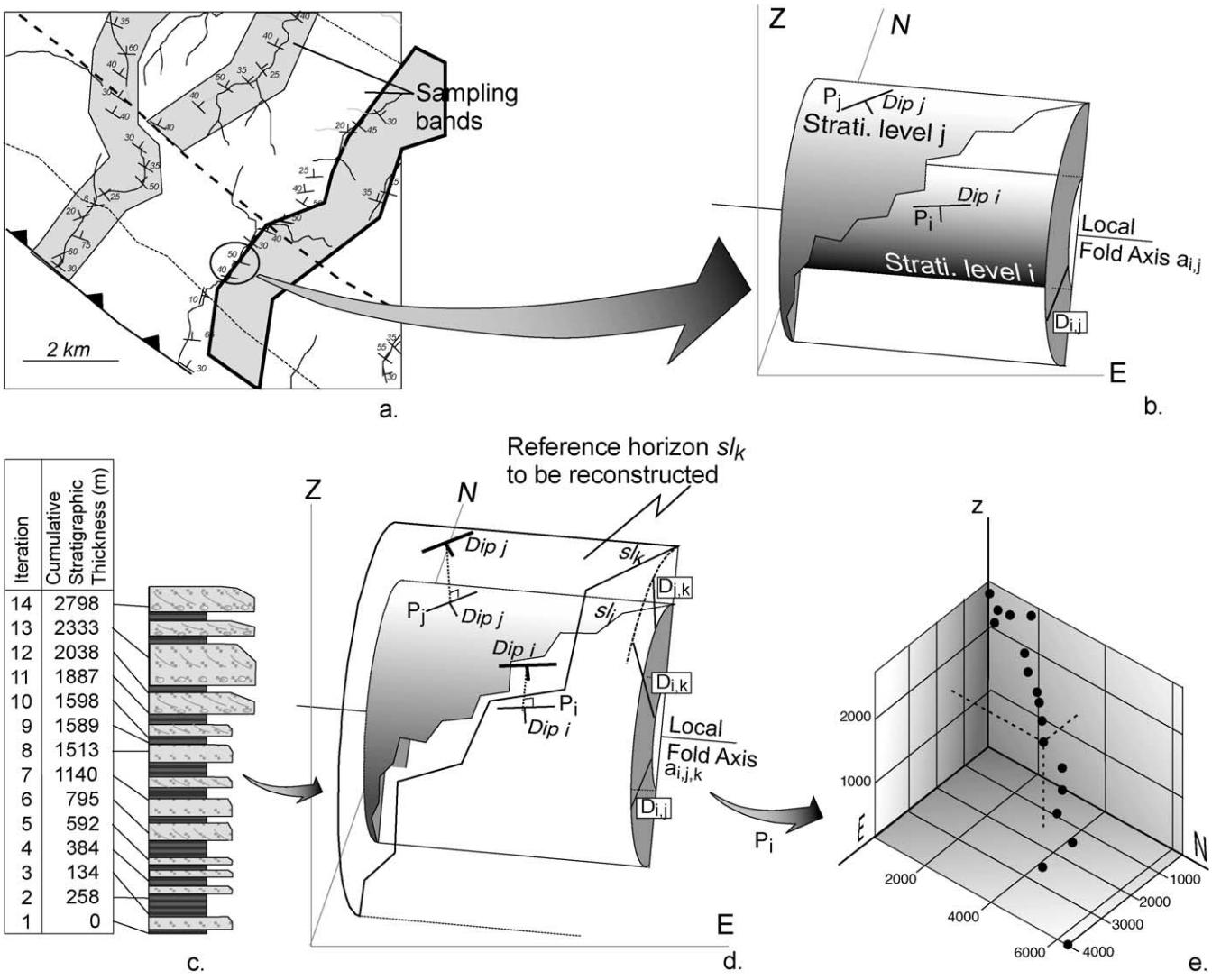

Fig. 4. (a) Sampling strategy for the structural data. Shaded areas are sampling bands, dotted lines are horizon intersections with the surface, dashed lines are the intersections of the reference horizons with the surface. Circled dots are a pair of points P_i and P_j for the next stage; (b) cylindration of the data pairs, where $D_{i,j}$ is the stratigraphic thickness between the data points P_i and P_j; and a_{ij} is the calculated local fold axis; (c) reconstruction of the thickness log corresponding to the cumulate elementary stratigraphic thicknesses for each pair of points; (d) projection of the elementary thicknesses along the poles of the strata. The inner shells ($s.l._i$ and $s.l._j$) are the strata on which structural measurements have been performed, the outer shell ($s.l._k$) is the reference horizon to be reconstructed. Bold dip symbols are the projected dots in space (from the measured strata), which belong to the reference horizon; (e) projection of the data from a sampling band: spatial coordinates of the projected dots.

bed N_i, defined by strikes and dips data from field measurements (Fig. 4a). It is subdivided into sub-sets along isopach sampling bands, striking across the structural trend. Each point belongs to one particular stratigraphic level (most of the time undetermined). The adjacent point within the 'band-section' belongs to another particular stratigraphic level, the strike and dip of which are not necessarily similar to the former. Datapoints can be regarded in pairs (P_i, P_j) in order to define the local folding attitude (Fig. 4b). The latter is assumed locally truly cylindrical. The two data P_i and P_j are considered as belonging to a pair of coaxial cylinders. Each cylinder tangents the bedding surface characterized by its normal N_i. For each pair (P_i, P_j), there is one and only one axis $a_{i,j}$ in space for both coaxial cylinders. The vector product $A_{i,j}$ of the normals N_i and N_j gives the axis orientation. The intersection of the two planes, respectively, defined by P_i, N_i and $A_{i,j}$ and P_j, N_j and $A_{i,j}$ gives the coordinates and location (ii) and trend and plunge (iii) of the cylinders axis $a_{i,j}$. The two radii of the aforesaid cylinders are the respective distances from the datapoints to the fold axis. The difference of these radii is the stratigraphic thickness $D_{i,j}$ between the two datapoints of the pair (iv).

The calculations of $D_{i,i+1}$ are performed successively along each 'band-section'. The total stratigraphic thickness along a sampling band is the sum of each elementary thickness value along the band (iv). This method accounts for both upward and downward calculation within the stratigraphic pile by addition or subtraction of the elementary

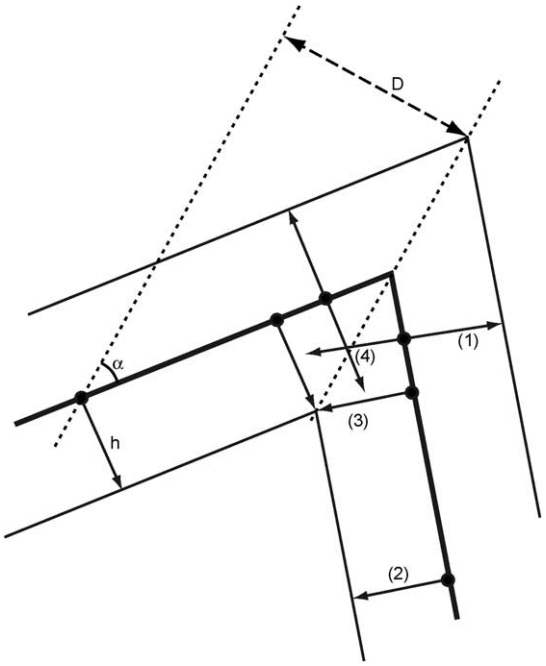

Fig. 5. Projections at the proximity of fold hinges. Dotted lines are bisectors of the kink. When the projection is directed from a horizon (bold) towards external shells (1) or when the source point is far enough from the fold hinge ($h \cos \alpha < D$) towards inner shells (2) and (3), the projections are correct. Where the source point is too close to the hinge ($h \cos \alpha > D$), the projected points are aberrant (4).

calculated thicknesses along a band. The cumulative stratigraphic thicknesses provide synthetic logs for each independent 'band-section' (Fig. 4c), which are parts of the total stratigraphic log of the area. Since no approximation has been done while calculating the thicknesses, the accuracy of the logs only depends on the initial data sets. Additional control is given from one flank to the other, as the cumulative thickness calculated by the projection series across one fold flank has to match with the cumulative thickness deduced from the other flank, otherwise it would generate discrepancies at the level of the hinge.

3.2. Spatial projection of the data sets

Reconstruction of the structure is performed by projecting the structural data onto chosen reference horizons. As the purpose is to characterize the geometry of the structure represented by these surfaces, their intersections with topography have to be accurately described, and particular attention must be paid to periclinal closures.

Once the cumulative stratigraphic thicknesses are calculated, the relative thicknesses $D_{i,j}$ from each datapoint to a reference horizon are assessed on the logs. The output datasets consist of the distances for each datapoint, from its particular strata to the reference horizon (v). Each initial datapoint P_i is projected, along the pole N_i from its original strata to the reference horizon at a distance $D_{i,j}$ (Fig. 4d).

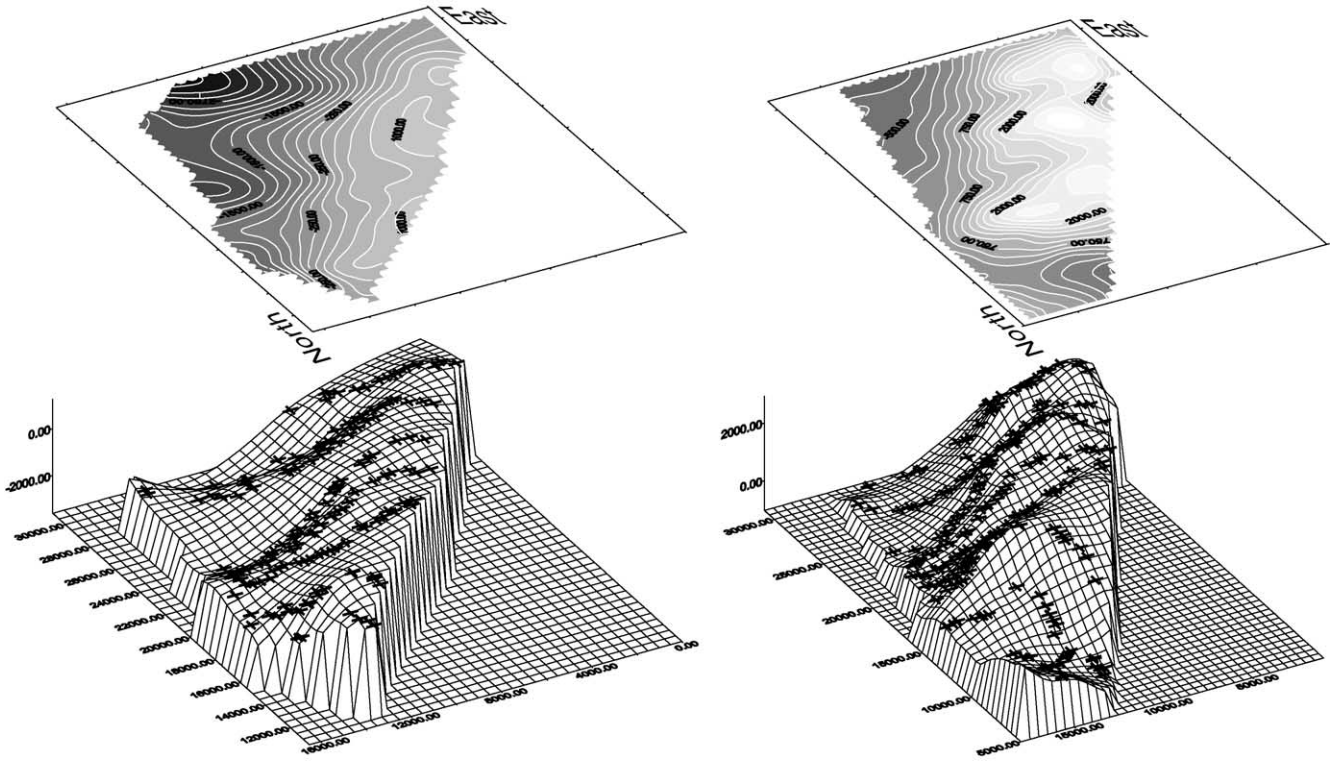

Fig. 6. Interpolated (kriging) reference horizons: MS1/MS2 boundary (left) and MS2/US1 boundary (right). Crosses are the projected structural data.

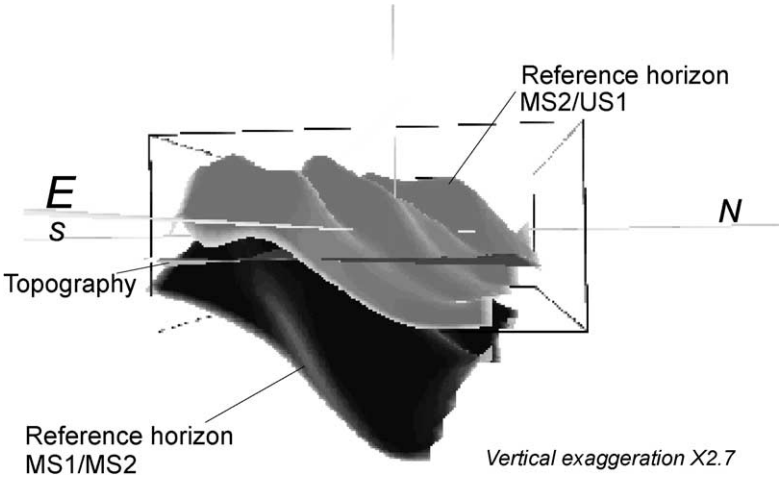

Fig. 7. 3D visualization of the reconstructed horizons with respect to topography.

According to the initial assumptions (flexural slip and constant bed thickness along a band), the resulting dots in space are located on a reference horizon. In fact, the spatial projections of these lengths for each particular 'band-section' define a band in space, which is included within the surface to be reconstructed (Fig. 4e).

Where the curvature is significant, artifacts can be generated. In order to avoid them, it has to be restricted to the cases illustrated in Fig. 5, where the distance D to the hinge is shorter than $h \cos \alpha$, where h is the interstrata thickness and α is the strata/hinge angle. It does not limit the technique to relatively open folds but only projections towards outer shells can be performed close to fold hinges when folds are tight.

This operation is successively realized for each sampling band, producing sets of dots defined by their coordinates, strikes and dips. These sets are located within the reference surfaces (vii). Subsequent interpolation of the data sets provides the 3D geometry of the structure.

4. 3D reconstruction and restoration of the Baisahi and Rapti folds

4.1. Reconstruction

The structural data set is divided into sampling bands, broadly perpendicular to the structural trend (Fig. 2). On the whole, these correspond to the drainage pattern where sampling has been done. As a consequence, the sub-sets comprise tight data within broadly parallel and linear 'band-sections'.

Processing of these sub-sets has to be carried out for each band, in order to reconstruct the two reference horizons between the Middle Siwaliks 1 (MS1) and Middle Siwaliks 2 (MS2) formations, and between the MS2 and Upper Siwaliks 1 (US1) formations. These reference surfaces have been chosen as they are well constrained from the structural analysis from fieldwork and SPOT imagery; moreover, they do not require many projections towards inner shells and artifacts close to fold hinges are avoided. Both horizons belong to the fold above the hanging-wall of the MFT and above the roof thrust of the duplex.

Following the method described above, two data sets (one per horizon) of projected dots are established. After projection, the output data sets are linked to the original map distribution of the input data sets. Interpolation is carried out by kriging. Details on the interpolation procedure can be found in Appendix A. Interpolation grids of the two reconstructed surfaces are represented in Fig. 6. The overall 3D visualization of the structural shape is given by both reference horizons with respect to topography (Fig. 7).

Both the buried part of the structure (Rapti syncline) and the eroded part of it (Baisahi antiform) are reconstructed in 3D. A slight pattern of thalwegs, perpendicular to strike, stands out and suggests that the fold axis varies along-strike. A detailed inspection of the dip and strike of the MS1/MS2 reference horizon in Fig. 2 confirms that the along-strike undulation appears in the initial data. Since the original distribution of the datasets has been accounted for while interpolating, and because the spatial distribution of the perpendicular to strike undulations does not particularly match the spatial distribution of the trends of the projected bands, it is assumed that this pattern reflects the real shape of the folded structure, though some artifacts cannot be locally excluded.

4.2. Unfolding

3D surfaces can be unfolded in order to test their validity and evaluate if they are developable. The reconstructed MS1/MS2 reference horizon is unfolded using Patchwork program (Bennis et al., 1991; Lecomte et al., 1994). The surface is gridded along isoparametric curves, then flattening is performed piecewise. Restoration is realized from a pin line by incremental flattening of the grid surface.

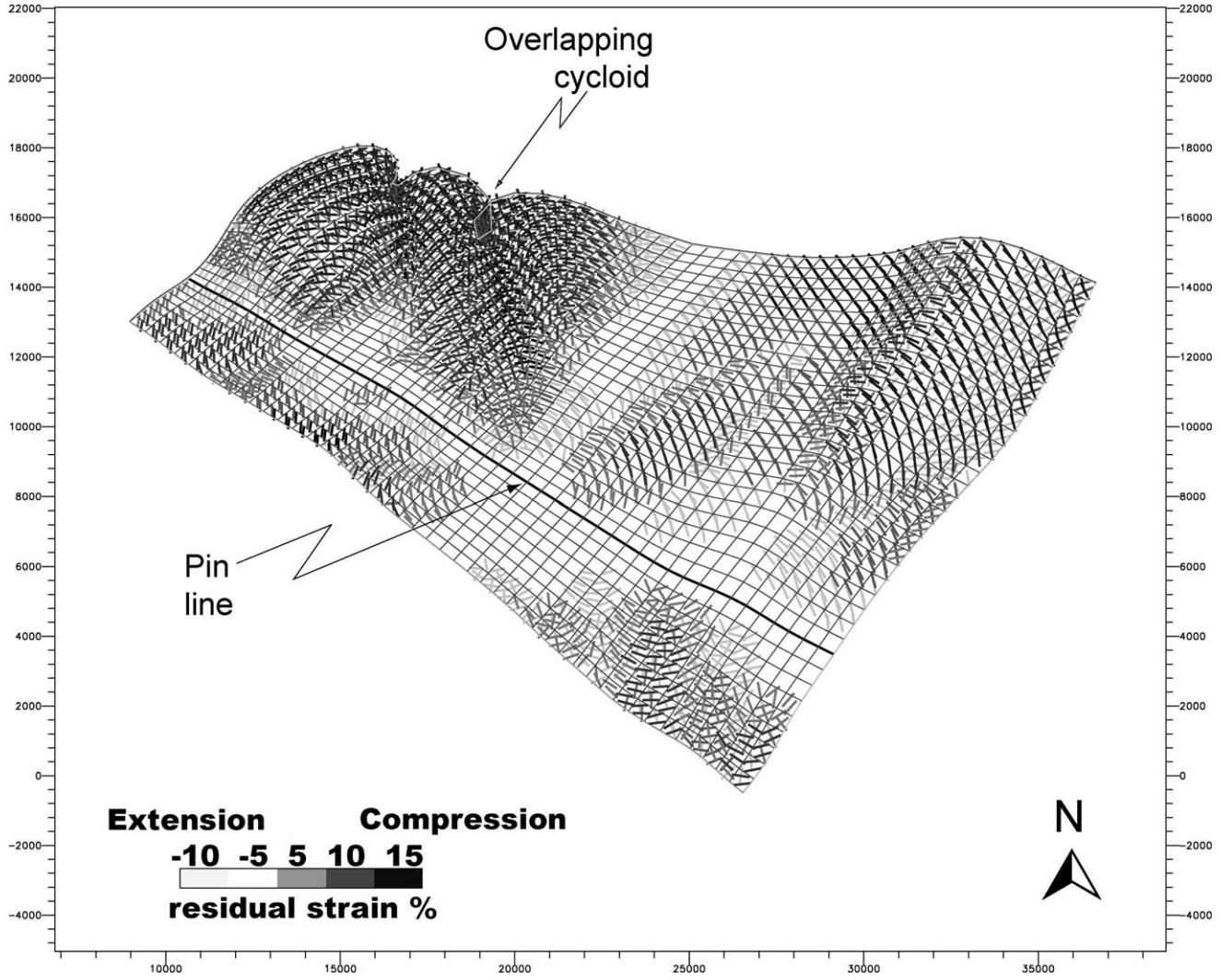

Fig. 8. Unfolded MS1/MS2 reference horizon. Compression and extension are given for the unfolding event. The overlapping cycloid is the representation of an extremely stretched area during folding. In such zones, the initial state cannot be restored; the residual strain field due to unfolding of the antiform measures the difference in shapes of the quadrangles in the folded structure and the flattened quadrangles.

Isoparametric curves of the deformed surface are mapped onto the flattening plane. Geodesic curvature, chords lengths and cross-angles are preserved. The flat quadrangles are recombined by means of rotation and translations, minimizing the misfits between pieces. Gentle distortion of the flattened quadrangles is applied to fill in the misfits (Bennis et al., 1991).

Assumption of pure flexural slip implies that the structure does not undergo major strain during the folding event. The studied structure is roughly cylindrical and shows slight deviations from true cylindricity (see stereoplot Fig. 2). The fold axis slightly undulates, as shown by the 3D view (Fig. 7). It is therefore globally developable (Lisle, 1992), and unfolding should then outline only local anomalies due to internal strain (including small-scale faulting and folding). The pin line is located at the fold crest, where layer-parallel shearing is assumed to be minimal (Suppe and Medwedeff, 1992). Distortion of the quadrangles is illustrated by the 'residual strain field' (Fig. 8), which corresponds to the 2D tensor of distortion required to fill in the misfit of the flattened quadrangles. It measures the differences of shapes between the initial and the final quadrangles. It either indicates local inaccuracy in the 3D surface or internal strain faulting. The NW and the NE zones, respectively, show W–E and NW–SE compressive distortion from the final to the initial state (i.e. during unfolding process). The distortion decreases in magnitude southward and is interpreted as an extensive internal strain hinterland during the lateral propagation of the structure from the initial to the final state. The unfolded MS1/MS2 horizon also features a little 'overlapping cycloid' at the NW of the surface, which is the representation of extremely distorted zones, above the threshold admitted by the program to shorten the pieces while filling in the misfits. It does not represent the actual unfolded state of the area but a local, significantly disturbed zone. Choosing a pin line in the cycloid would significantly

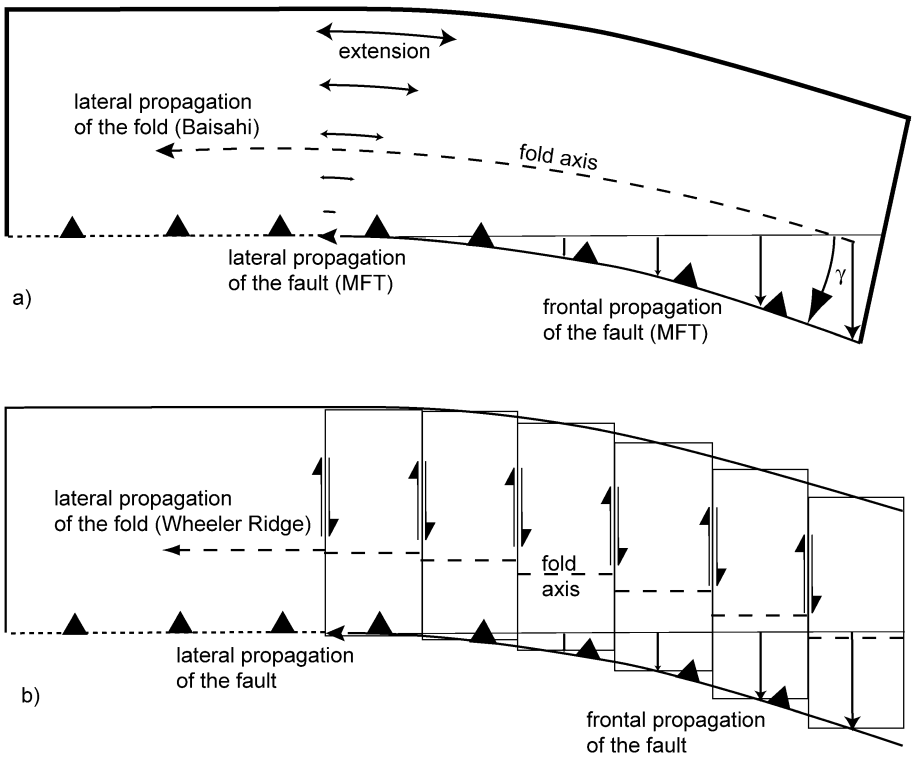

Fig. 9. Hinterland extension induced by the lateral propagation of a structure. (a) Internal strain, Baisahi fold. While the mature part of the structure (right) continues to evolve, along-strike extension is induced on the trailing edge of the fold, accommodated by internal strain. γ is the rotation angle between the mature (right) and immature (left) parts of the structure (20° for the Baisahi anticline). (b) Tear faults, Wheeler Ridge type (after Medwedeff, 1992; Mueller and Talling, 1997). The displacement gradient is there accommodated by block segmentation.

modify the results of the unfolding procedure, although it would not erase the high residual strain in the NW area. To the NW, minor accommodation faults are mapped, west of the cycloid, also indicating that this area underwent high shear strains.

4.3. Discussion

As the thrust propagates southward and westward, there is a rotation of at least 20° clockwise, which induces a shear component hinterland, where the synclinal breakthrough is not initiated yet. It can be accommodated either by hinterland extension (Fig. 9a) or tear faults, parallel to the main shortening axis (e.g. Mueller and Talling, 1997; Fig. 9b). No tear fault has been evidenced in this area from field work and SPOT imagery; this suggests a diffuse shear strain accommodation rather than tear faults, which is furthermore supported by the hinterland compression in the residual strain field (Fig. 8). This mechanism also suggests that shortening is not parallel to the main horizontal stress at the transition between monocline and anticline. However, as soon as this zone propagates laterally, shortening becomes parallel to the main stress axis again.

According to the residual strain field, less than 1 km of shortening is accommodated by internal strain along a cross-section, whereas the total shortening is more than 15 km. Since the differences between regional folding and internal strain are of more than one order of magnitude, we emphasize that in a first order approximation, hinterland along-strike extension does not affect significantly the 2D reconstruction. However, the stratigraphic thicknesses can change laterally. It has been shown that the roof rotates around the migrating Baisahi western pericline, making the motion of the roof slightly oblique to across-strike sections. As the thicknesses appear to change along-strike, they can slightly differ below and above the MFT, making the 3D reconstruction more valid than the 2D sections.

Mueller and Talling (1997) showed that the Wheeler Ridge fold is truly cylindrical. Furthermore, the shear component seems mainly accommodated by tear faults. On the contrary, the Baisahi anticline is not truly cylindrical since its axis undulates and finally plunges towards the NW. In that case, the shear component seems mainly accommodated by internal strain rather than tear faults (Fig. 9). If it is assumed that the internal strain is mainly induced by a simple shear direction of no finite longitudinal extension parallel to the regional transport direction, it would bring about a principal finite extension orientated nearly NNW–SSE to N–S. Furthermore, since a component of extension parallel to the fold axe is described in numerous fold belts (Vialon et al., 1984), an additional NW–SE extension is inferred at the trailing edge of the Baisahi anticline.

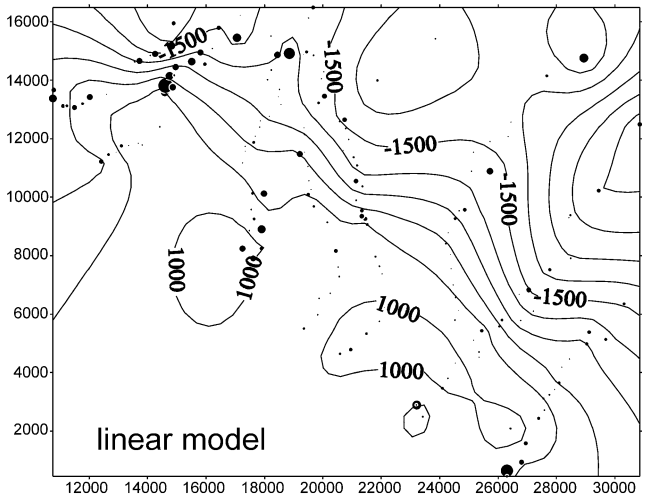

Fig. 10. Geographical repetition of the residuals after interpolation. The distribution is indicated by filled circles; diameter is proportional to the absolute value of the residual. The greatest circle is 250 m. Coordinates are in meters. Elevation in meters above sea level. Parameters of the kriged surface: grid spacing 200 m; linear model: nugget 70; anisotropy ratio 2 in the N105 direction; scale: 1×10^6; length: 12900.

5. Conclusions

The main purpose of the study was to develop an original 3D reconstructing method from outcrop data. This method based on a flexural slip hypothesis is well adapted to fold and thrust belts and may be useful in remote areas of frontal parts of orogenic belts where no subsurface data are available to constrain the geometry of the structures. This technique allows one to reconstruct both the eroded and buried parts of the structures.

By reconstructing two surfaces defined over the Main Frontal Thrust from combined structural fieldwork and spatial imagery, the 3D shape of the eroded Baisahi antiform and the preserved Rapti syncline are characterized with respect to the topography. It has been shown, by the example of the Baisahi anticline, that deformation in fold and thrust belts can deviate from true cylindrical patterns. Since lateral thickness variations are present in many natural settings, additional deviations from a truly cylindrical structure are generated and are accounted for in our method. Hence, this 3D reconstruction technique provides a more accurate description of the shape of the structure than 2D reconstruction.

Additionally, 3D restoration of a reference horizon of the Baisahi antiform has been carried out using Patchwork program in order to test a reconstructed surface. In spite of the globally cylindrical (and hence potentially developable) shape of the structure, unfolding revealed along-strike stretched zones. Bulk shear and extensional internal strain rather than tear faults accommodate the rotation of the hanging wall around the migrating fold pericline.

Acknowledgements

This work was funded by the INSU program PROSE: Himalayan erosion. The manuscript has greatly benefited from reviews by D. Rouby and K. Mueller. We also thank F. Roure for constructive discussions.

Appendix A. Description of the interpolation procedure and parameters

The nugget effect (*Nu*) has been estimated from the data repeatability: the uncertainty for the geographic position (*Po*) is in the order of 20 m, the uncertainty on the measurement of the normal to the bedding plane ($\delta\alpha$) is 5° and the mean distance of projection (dist) is 600 m. Therefore the nugget effect is about $Po + \sin(\delta\alpha) \times \text{dist}$, i.e. 70 m. The grid spacing is 200 m. In order to counteract the anisotropic distribution of dots in space and to outline the general trend of the structure, relative weighting has been defined by an anisotropy ratio of two in the N105 direction. The variogram is based on a linear model, with the default parameters proposed by Surfer interpolator (Golden Software, IC). Several other interpolation procedures have been tested but the results do not strongly differ from the result of the linear one. The standard deviation of the residuals between the data and the kriged surface is 62 m and the maximum residual is 250 m. The geographical distribution of the residuals is shown in Fig. 10 by filled circles.

References

Acharyya, S.K., 1994. The Cenozoic foreland basin and tectonics of the eastern Sub-Himalaya: prospects and problems. Himalayan Geology 15, 3–21.

Appel, E., Rosler, W., 1994. Magnetic polarity stratigraphy of the Neogene Surai Khola section (Siwalik, SW Nepal). Himalayan Geology 15, 63–68.

Baby, P., Hérail, G., Salinas, R., Sempere, T., 1992. Geometry and kinematics of passive-roof duplexes deduced from cross-section balancing: example from the foreland thrust system of the southern Bolivian Subandean Zone. Tectonics 3, 523–536.

Banks, C., Warburton, J., 1986. "Passive-roof" duplex geometry in the frontal structures of the Kirthar and Sulaiman mountain belts, Pakistan. Journal of Structural Geology 8, 229–237.

Bennis, C., Vézien, J.M., Iglesias, G., 1991. Piecewise surface flattening for non-distorted texture mapping. Computer Graphics 4, 237–246.

Bilham, R., Larson, K., Freymueller, J., 1997. Idylhim members. GPS measurements of present-day convergence across the Nepal Himalaya. Nature 386, 61–63.

Biswas, S.K., 1994. Status exploration for hydrocarbons in Siwalik basin of India and future trends. Himalayan Geology 15, 283–300.

Boyer, S., 1986. Styles of folding within thrust sheets: examples from the Appalachian and Rocky Mountains of the USA and Canada. Journal of Structural Geology 8, 325–339.

Boyer, S.E., Elliott, D., 1982. Thrust systems. American Association of Petroleum Geologists Bulletin 66, 1196–1230.

Busk, H., 1929. Earth Flexures. Cambridge University Press 186pp.

Coward, M.P., Potts, G.J., 1983. Complex strain patterns developed at the

frontal and lateral tips to shear zones and thrust zones. Journal of Structural Geology 5, 383–399.
Dahlstrom, C.D.A., 1969. Balanced cross-sections. Canadian Journal of Earth Sciences 6, 743–757.
Delcaillau, B., 1997. Les fronts de chaÎne actives—Genèse des reliefs et relations tectonique-érosion-sédimentation. Thèse d'habilitation à diriger des recherches, Université de Caen.
De Mets, C., Gordon, R.G., Argus, D.F., Stein, S., 1990. Current plate motions. Geophysical Journal International 101, 425–478.
Galahaut, V.K., Chandler, R., 1992. On the active tectonics of the Dehra Dun region from observations of ground elevation changes. Journal of the Geological Society of India 39, 61–68.
Hérail, G., Mascle, G., 1980. Les Siwaliks du Népal Central: structures et géomorphologie d'un piedmond en cours de déformation. Bulletin de l'Association Géographique Française 431, 259–267.
Hérail, G., Mascle, G., Delcaillau, B., 1987. Les Siwaliks de l'Himalaya du Népal: un exemple de prisme d'accrétion intracontinental in S.D.L.T.P., Bordet 47, 153–182.
Husson, L., Mugnier, J.L., Leturmy, P., Vidal, G., 2002. Frontal development of the Himalayas: sedimentary record and architecture of the Siwaliks of Western Nepal. In: McClay, K. (Ed.), Thrust Tectonics and Hydrocarbon Systems, AAPG Memoir, in press.
Jackson, M., Bilham, R., 1994. Constraints on Himalayan deformation inferred from vertical velocity fields in Nepal and Tibet. Journal of Geophysical Research 99, 13,897–13,912.
Jouanne F., Mugnier, J.-L., Pandey, M.R., Gamond, J.-F., Le Fort, P., Serrurier, L., Vigny, C., Avouac, J.P., Idylhim members, 1999. Oblique convergence in Himalaya of western Nepal deduced from GPS measurements, 14th Himalaya–Karahorum–Tibet Workshop, Tubingen.
Kayastha, N.B., Pradhan, U.M., Shresta, R.B., Shyam, K.C., Subedi, D.N., Sharma, S., 1999. Geological map of exploration block-3 Nepalganj, Mid-Western, Nepal, Department of Mines and Geology, Kathmandu.
Lavé, J., Avouac, J.-P., 2000. Active folding of fluvial terraces across the Siwaliks Hills, Himalayas of central Nepal. Journal of Geophysical Research 105, 5735–5770.
Lecomte, J.-C., Mondy, J.-F., Bennis, C., Léger, M., 1994. A Balanced Surface Method. A New Way to Improve your Structural Maps Interpretations. AAPG Convention, Denver.
Leturmy, P., 1997. Sédiments et reliefs du front des systèmes chevauchants: Modélisation et exemples du front Andin et des Siwalik à l'Holocène. PhD thesis, Université Joseph Fourier, Grenoble I.
Lisle, R.J., 1992. Constant bed-length folding: three dimensional geometrical implications. Journal of Structural Geology 14, 245–252.
Lyon-Caen, H., Molnar, P., 1985. Gravity anomalies, flexure of the Indian plate, and the structure, support and evolution of the Himalaya and Ganga basin. Tectonics 4, 513–538.
Mascle, G., Hérail, G., Van Haver, T., Delcaillau, B., 1986. Structure et évolution des bassins d'épisuture et de périsuture liés à la chaÎne himalayenne. Société Nationale Elf Aquitaine Production, Bull. Centre Rech. Explor-Prod. 10, 181–203.
Medwedeff, D.A., 1992. Geometry and kinematics of an active laterally propagating wedge thrust, Wheeler Ridge, California. In: Mitra, S., Fisher, G.W. (Eds.), Structural Geology of Fold and Thrust Belts, The John Hopkins Studies in Earth and Space Sciences 5, pp. 1–28.
Molnar, P., Tapponnier, P., 1975. Cenozoic tectonics of Asia: effects of a continental collision. Science 189, 419–426.
Mueller, K., Talling, P., 1997. Geomorphic evidence for tear faults accommodating lateral propagation of an active fault-bend fold, Wheeler Ridge, California. Journal of Structural Geology 19, 397–411.
Mugnier, J.-L., Mascle, G., Faucher, T., 1992. La structure des Siwaliks de l'Ouest Népal: un prisme d'accrétion intracontinental. Bulletin de la Société Géologique de France 163, 585–595.
Mugnier, J.-L., Huyghe, P., Chalaron, E., Mascle, G., 1994. Recent movements along the Main Boundary Thrust of the Himalayas: normal faulting in an over critical thrust wedge? Tectonophysics 238, 199–215.
Mugnier, J.-L., Delcaillau, B., Huyghe, P., Leturmy, P., 1998. The breakback thrust splay of the Main Dun Thrust: evidence of an intermediate displacement scale between earthquake slip and finite geometry of thrust systems. Journal of Structural Geology 20, 857–864.
Mugnier, J.-L., Leturmy, P., Mascle, G., Huyghe, P., Chalaron, E., Vidal, G., Husson, L., Delcaillau, B., 1999. The Siwaliks of Western Nepal. I. Geometry and kinematics. Journal of Asian Earth Sciences 17, 629–642.
Ni, J., Barraganzi, M., 1996. Seismotectonics of the Himalayan collision zone: geometry of the underthrusting Indian plate beneath the Himalaya. Journal of Geophysical Research 89, 1147–1163.
Peltzer, G., Saucier, F., 1996. Present-day kinematics of Asia derived from geologic fault rates. Journal of Geophysical Research 101, 27,943–27,956.
Powers, P.M., Lillie, R.J., Yeats, S., 1998. Structure and shortening of the Kangra and Dehra Dun reentrants, Sub-Himalaya, India. Geological Society of America Bulletin 110, 1010–1027.
Price, R.A., 1981. The Cordilleran fold and thrust belt in the southern Canadian Rocky Mountains. In: McClay, K., Price, N.J. (Eds.), Thrust and Nappe Tectonics, Geological Society Special Publication 9, pp. 427–448.
Raiverman, V., Srivastava, A.K., Prasad, D.N., 1994. Structural style in north-western Himalayan foothills. Himalayan Geology 15, 263–280.
Schelling, D., 1992. The tectonostratigraphy and structure of the eastern Nepal Himalaya. Tectonics 11, 925–943.
Schelling, D., Arita, K., 1991. Thrust tectonics, crustal shortening, and the structure of the far-eastern Nepal Himalaya. Tectonics 15, 851–862.
Srivastava, P., Mitra, G., 1994. Thrust geometries and deep structure of the outer and lesser Himalaya, Kumaon and Garhwal (India): implications for evolution of the Himalayan fold and thrust belt. Tectonics 13, 89–109.
Storti, F., Salvini, F., 1996. Progressive rollover fault-propagation folding: a possible kinematic mechanism to generate regional-scale recumbent folds in shallow foreland belts. Bulletin of the American Association of Petroleum Geologists 80, 174–193.
Suppe, J., 1980. Imbricated structure of western foothills belt, southern central Taiwan. Petroleum Geology Taiwan 17, 1–16.
Suppe, J., Medwedeff, D.A., 1990. Geometry and kinematics of fault-propagation folding. Eclogae Geologicae Helveticae 83, 409–454.
Vann, I.R., Graham, R.H., Hayward, A.B., 1986. The structure of mountain fronts. Journal of Structural Geology 8, 215–227.
Vialon, P., Bonnet, J.L., Gamont, J.F., Mugnier, J.L., 1984. Modélisation des déformations d'une série stratifiée par le déplacement horizontal d'un poinçon. Bulletin de la Société Géologique de France 26, 139–150.
Wines, R.F., 1990. Productive duplex imbrication at the Neuquén basin thrust belt front, Argentina. In: Letouzey, J. (Ed.). Petroleum and Tectonics in Mobile Belts. Technip, Paris, pp. 69–80.
Woodward, N.B., Boyer, S.E., Suppe, J., 1985. An outline of balanced cross-sections. Studies in Geology 11. Department of Geological Sciences, University of Tennessee, Knoxville, 170pp.